Slopes, nearly constant loss, universality, and hopping rates for dispersive ionic conduction

2007 J. Phys.: Condens. Matter 19 046215

(http://iopscience.iop.org/0953-8984/19/4/046215)

INSTITUTE OF PHYSICS PUBLISHING JOURNAL OF PHYSICS: CONDENSED MATTER

J. Phys.: Condens. Matter **19** (2007) 046215 (13pp) doi:10.1088/0953-8984/19/4/046215

Slopes, nearly constant loss, universality, and hopping rates for dispersive ionic conduction

J Ross Macdonald[1] **and Mohamad M Ahmad**[2]

[1] Department of Physics and Astronomy, University of North Carolina, Chapel Hill, NC 27599-3255, USA
[2] Department of Science and Mathematics, Faculty of Education, Assiut University Branch in the New Valley, El-Kharga 72511, Egypt

E-mail: macd@email.unc.edu

Received 7 October 2006
Published 12 January 2007
Online at stacks.iop.org/JPhysCM/19/046215

Abstract

The title topics are investigated, discussed, and new insights provided by considering isothermal frequency response data for seven different materials having quite different conductivity spans and involving different electrode polarization effects and temperatures. These data sets were fitted using several different models, including the Kohlrausch-related K0 and K1 ones derived from stretched-exponential response in the temporal domain. The quasi-universal UN model, the K1 with its shape parameter, β_1, fixed at $1/3$, fitted most of the data very well, and its fits of such data were used to compare its predictions for hopping rate with those derived from fitting with the conventional 'universal dynamic response' Almond–West real-part-of-conductivity model. The K1-model theoretical hopping rate, involving the mean waiting time for a hop and derived from microscopic stochastic analysis, was roughly twice as large as the empirical Almond–West rate for most of the materials considered and should be used in place of it. Its use in a generalized Nernst–Einstein equation led to comparison of estimates of the concentration of fully dissociated mobile charge carriers in superionic $PbSnF_4$ with earlier estimates of Ahmad using an Almond–West hopping rate value. Agreement with an independent structure-derived value was relatively poor. Fitting results obtained using the K0 model, for Na_2SO_4 data sets for two different polycrystalline material phases, and involving severely limited conductivity variation, were far superior to those obtained using the K1 model. The estimated values of the K0 shape parameter, β_0, were close to $1/3$ for both phases, strongly suggesting that the charge motion was one dimensional for each phase, even though they involved different crystalline structures.

1. Background

Fitting and analysis of dispersive frequency response data are essential in establishing valid identifications and interpretation of the physical processes associated with such data. But the use of physically inappropriate and improper data fitting models, even when they fit the data adequately, can yield misleading conclusions, and the damage is compounded when the users of such models are unaware of their deficiencies, frequently the case. Therefore, in recent years much effort has been devoted by one of the present authors (JRM) to evaluating and critiquing several popular models proposed to represent the dispersed frequency response of ionic conductors, especially thermally activated ones.

In particular, the following models have been considered, problems identified, and superior approaches or corrections discussed in the references cited.

(a) The 1973 original widely used modulus formalism (OMF) fitting model of Moynihan and associates [1–3]. Although it is inappropriate, it is still used. See the discussion in section 2 of its use of the K1 model.
(b) The 1979 Ngai coupling model and its superior alternative, the cut-off model [2, 4]. The cut-off model can lead to the usual activation-energy relation of the coupling model but it is physically much more plausible than is the latter [2].
(c) The Funke mismatch and relaxation model [5, 6]. It involves forward and backward hopping.
(d) Power-law models: universal dynamic response, the ZC model, and the Almond–West (AW) model [7, 8].
(e) Series and parallel model additions: nearly constant loss (NCL) and electrode polarization effects [3, 9, 10].

It is important to distinguish between models appropriate for dielectric situations, where the dipolar dielectric response, $\varepsilon_{\mathrm{D}}(\omega)$, is distributed and involves a distribution of dielectric relaxation times, and conductive-system ones, where the resistivity, $\rho(\omega)$, involves a distribution of resistivity relaxation times. For example, the use of the Cole–Cole response function [11] at the dielectric level leads to dispersed dielectric response while its use as a model at the impedance level, then called the ZC or ZARC model, yields dispersed conductive-system response [8]. Clearly, just transforming Cole–Cole response from the dielectric level to the resistivity level is not equivalent to ZC response and vice versa.

The analyses listed above and the present work deal primarily with conductive-system dispersion situations. In discussing the subjects of the title, we will deal particularly with the K1 and K0 models, derived from stretched-exponential behaviour in the temporal domain; with the power-law models listed in (d) above; and with composite fitting models that include both a dispersive bulk response model and an additional model electrically in series or parallel with it, as mentioned in (e). It will be shown that, contrary to earlier assumptions, a theoretically well based estimate of the mean hopping rate of ions can be identified, and its values will be compared, for a wide variety of data, with those following from the empirical Almond–West approach for estimating such rates.

2. Data, models, and fits

Figure 1 shows $\sigma'(\omega)$ responses for seven different materials, identified and referenced in table 1. These results are consistent with the usual finding that the conductivity range of such data, expressed in decades and defined as $D_\sigma \equiv \log_{10}(\sigma'_{\mathrm{max}}/\sigma_0)$ or just $\log_{10}(\sigma'/\sigma_0)$, rarely exceeds three decades except in exceptional cases such as that presented in [19]. Here

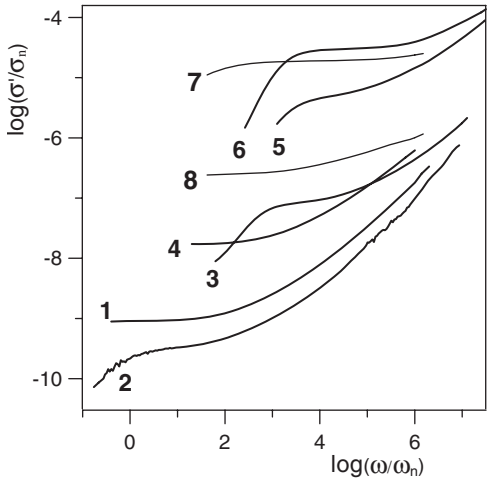

Figure 1. Log–log plots of experimental $\sigma'(\omega)$ frequency responses for seven different materials, identified in table 1. Here the normalization quantity ω_n is 1 r s^{-1} and σ_n is 1 S cm^{-1}.

$\sigma_0 \equiv \sigma'(0) = 1/\rho_0$. Fitting and parameter estimate results for the eight data sets of figure 1 are listed in table 1, where only a few fits of the full complex data are included. The fitting models used are described below. By restricting attention to fitting of only the real part of the data expressed at the complex conductivity level, $\sigma'(\omega)$, the effects of the high-frequency-limiting bulk dielectric constant of the material, $\varepsilon_{D\infty} \equiv \varepsilon'_D(\infty)$, do not appear and there is then no difference between fits using the erroneous OMF approach [12] and its corrected version [1–3, 20].

The fitting models employed to obtain the results shown in table 1 are, in order of increasing complexity:

- The series constant phase element, SCPE, called S here,

$$\sigma_{SC}(\omega) \equiv \varepsilon_V A_{SC}(i\omega)^{\gamma_{sc}}, \qquad \text{with } 0 < \gamma_{SC} \leqslant 2. \tag{1}$$

- The series SC_p, defined as the SCPE and a dielectric constant ε_p representing a capacitance in parallel with it,

$$\sigma_{SC_p}(\omega) \equiv \sigma_{SC}(\omega) + i\omega\varepsilon_V\varepsilon_p. \tag{2}$$

- The Almond–West model,

$$\sigma_{AW} = \sigma'_{AW} \equiv \sigma_0[1 + (\omega\tau_{AW})^n] \equiv \sigma_0[1 + (\omega/\omega_{AW})^n]. \tag{3}$$

- The ZC model,

$$\sigma_{ZC} \equiv \sigma_0[1 + (i\omega\tau_{ZC})^n]. \tag{4}$$

- Models derived from stretched-exponential response in the temporal domain: the K0, K1, and UN ones [1–3, 20] involve the shape parameters β_0, β_1, and $\beta_1 = 1/3$ which satisfy the conditions $0 < \beta_k \leqslant 1$, where $k = 0$ or 1. The UN model is just a simplification of the K1, one with the value of β_1 fixed at 1/3 and marked 1/3 F in the table. The characteristic relaxation times of the K0 and K1 models are denoted as τ_{Ck}, where the subscript C indicates conductive-system response.

Table 1. Fit results for the seven different materials of figure 1. All fits are of $\sigma'(\omega)$ data sets except the CUNS, CK1S, and CK0S ones, which are fits of the full $\sigma(\omega)$ data. $100S_F$ is the per cent relative standard deviation of the residuals of a fit. Brackets [ ], are used to distinguish different situations, and braces { }, designate very poorly determined results. In Kk, $\langle\tau\rangle$ and β_k, $k = 0$ or 1. D_σ is the number of decades from $\sigma_0 \equiv 1/\rho_0$ to σ'_{max}. Here, $\langle\tau\rangle$ is $\langle\tau\rangle_{01}$ for the K1 and UN models or $\langle\tau\rangle_0$ for the KO one; τ_C is either τ_{ZC} or τ_{AW}; and $r_R \equiv \tau_C/\langle\tau\rangle_{01}$, with its value in parentheses when K1 rather than UN values of $\langle\tau\rangle_{01}$ are used.

# Material (ref.); D_σ	T (K)	Model	$100S_F$	ρ_0 (Ω cm)	$\langle\tau\rangle$ [τ_C] (s)	β_k [n]	r_R
1 $Li_2O{\cdot}Al_2O_3{\cdot}2SiO_2$ [12] 2.3;	297	CUNS	2.36	1.088×10^9	2.610×10^{-4}	1/3 F	
		UNS	2.58	1.095×10^9	2.744×10^{-4}	1/3 F	
		K1S	2.63	1.094×10^9	2.847×10^{-4}	0.337	
		ZCS	1.82	1.148×10^9	$[1.105 \times 10^{-3}]$	[0.640]	
		AWS	1.83	1.147×10^9	$[4.161 \times 10^{-4}]$	[0.640]	1.52
2 $CsPO_3$ [13]; 3.3	298	$UNSC_p$	4.08	2.925×10^9	3.252×10^{-4}	1/3 F	
		$ZCSC_p$	3.95	3.177×10^9	$[1.480 \times 10^{-3}]$	[0.611]	
		$AWSC_p$	3.97	3.284×10^9	$[6.470 \times 10^{-4}]$	[0.613]	1.99
3 $0.4AgI{\cdot}0.6(0.5Ag_2O_3{\cdot}0.5MoO_3)$ [14]; 1.4	143	UNS	2.70	1.056×10^7	5.355×10^{-6}	1/3 F	
		ZCS	2.89	1.151×10^7	$[2.458 \times 10^{-5}]$	[0.650]	
		AWS	2.82	1.212×10^7	$[1.005 \times 10^{-5}]$	[0.650]	1.88
4 $0.88ZrO_2{\cdot}0.12Y_2O_3$ [15]; 1.6 (single crystal)	503	UNS	0.74	5.793×10^7	3.047×10^{-5}	1/3 F	
		K0S	0.86	5.484×10^7	1.927×10^{-4}	0.553	
		ZC	1.64	6.240×10^7	$[1.380 \times 10^{-4}]$	[0.619]	
		AW	1.64	6.240×10^7	$[5.457 \times 10^{-5}]$	[0.619]	1.79
5 $0.5Li{\cdot}0.5La{\cdot}TiO_3$ [16]; 2.3	225	UNS	0.86	1.811×10^5	2.604×10^{-7}	1/3 F	
		ZCS	1.01	2.096×10^5	$[1.411 \times 10^{-6}]$	[0.596]	
		AWS	0.93	2.260×10^5	$[7.265 \times 10^{-7}]$	[0.583]	2.79
6 $PbSnF_4$ [17]; 0.68	262	UNS	1.36	3.345×10^4	1.577×10^{-7}	1/3 F	
		K1S	1.30	3.327×10^4	$[2.541 \times 10^{-7}]$	0.387	
		K0S	1.31	3.317×10^4	$[1.173 \times 10^{-6}]$	0.538	
		ZCS	1.78	3.467×10^4	$[6.857 \times 10^{-7}]$	[0.661]	
		AWS	1.73	3.497×10^4	$[2.518 \times 10^{-7}]$	[0.657]	(0.99)
7 Na_2SO_4 [18]; 0.12	540	CK1S	1.16	5.190×10^4	$\{5.8 \times 10^{-10}\}$	0.173	
		K1S	0.34	5.173×10^4	$\{4.8 \times 10^{-10}\}$	0.169	
		CK0S	1.13	5.186×10^4	1.75×10^{-7}	0.333	
		K0S	0.21	5.191×10^4	1.99×10^{-7}	0.322	
		ZCS	0.32	5.245×10^4	$[6.359 \times 10^{-8}]$	[0.691]	
		AWS	0.32	5.249×10^4	$[2.110 \times 10^{-8}]$	[0.691]	
8 Na_2SO_4 [18]; 0.68	461	CK0S	1.86	3.987×10^6	4.71×10^{-5}	0.336	
		K0S	1.07	4.123×10^6	7.57×10^{-5}	0.316	
		K0	2.00	4.110×10^6	7.47×10^{-5}	0.318	
		ZC	2.39	4.606×10^6	$[8.89 \times 10^{-6}]$	[0.378]	
		AW	2.39	4.606×10^6	$[5.41 \times 10^{-6}]$	[0.378]	

In equations (1) and (2), ε_V is the permittivity of vacuum. Although Kk models cannot be expressed in closed form except for the fractional β_k values 1/3, 1/2, and 2/3, their frequency dependences may be very accurately calculated in the range $0.15 \leqslant \beta_k \leqslant 0.75$. Their responses are instantiated in the freely available, complex-nonlinear-least-squares (CNLS) fitting, simulation, and inversion program LEVM [21].

In 1973, Moynihan and co-authors published a macroscopic derivation of the K1 model [12], one that invoked a stretched-exponential Kohlrausch temporal response,

$\phi(t) = \exp[-(t/\tau_{C0})^{\beta_0}]$. Some vagaries of this derivation are discussed in [3]. An independent contemporaneous microscopic continuous-time random-walk-on-a-lattice derivation by Scher and Lax [22] eventually also led to conductive-system K1 response [6], as explained below. This fully microscopic model includes both forward and backward hopping.

The Scher–Lax stochastic transport model (STM) involved a general expression for $\phi(t)$, defined as the probability that a mobile charge remains fixed in the interval $[0, t]$. Although temporal and frequency responses associated with the choice of some specific choices for $\phi(t)$ were included in this work, the stretched exponential was not one of them. In the Scher–Lax STM derivation, the mean time for a hop, the mean waiting time, is given by $\langle\tau\rangle \equiv \int_0^\infty \phi(t)\,\mathrm{d}t$, leading, for the K1 model, to the $\langle\tau\rangle_{01}$ quantity of equation (5).

The K1 model is particularly important because it is the only response model that has been derived from both macroscopic and microscopic physical considerations [12, 22]. In addition, it has been shown, using constraint theory, that for hopping in three dimensions in microscopically homogeneous materials its β_1 shape parameter should have a semi-universal value of $1/3$, independent of temperature and ion concentration [20, 23]. The resulting model has been termed the UN one and has been found to fit frequency response data for a wide variety of materials with mobile charges of a single type [1–3, 10]. To avoid the inconsistency of the inappropriate OMF model [1, 3, 20], however, such fitting generally requires the inclusion of a free parameter representing the limiting high-frequency bulk dielectric constant $\varepsilon_{D\infty}$, leading to the CK1 and CUN composite models.

In order for the Scher–Lax STM model to be identical to the K1 one, its $\phi(t)$ must be a stretched-exponential function. In the 1996–1997 work of [24] and [25], not only were defects in the OMF pointed out but also synthetic and experimental data sets were fitted with K1 and CK1 models, ones derived from stretched-exponential temporal response. But, as shown in [6], submitted in 2000, the STM is only fully identical to the K1 when a high-frequency correction is made to it. Although its response, expressed at the complex dielectric constant level, involves an expression for $\varepsilon''_{STM}(\omega)$ identical with that for the K1, its $\varepsilon'_{STM}(\omega)$ part lacks the high-frequency-limiting conductive-system effective dielectric constant $\varepsilon_{C1\infty}$ because the STM is a low-frequency theory [6]. Nevertheless, it was shown, by means of a distribution of relaxation times deconvolution approach, that consistency with its $\varepsilon''_{STM}(\omega)$ response required the addition of $\varepsilon_{C1\infty}$ to its $\varepsilon'_{STM}(\omega)$ part [6]. The extended STM is then isomorphic with the K1.

In table 1, only UNS fit results are included for those cases where K1S-model fits led to β_1 estimates very close to $1/3$. The UNS model has been used because of its generality, its strong theoretical justification, and its ability to fit the data better than alternative models such as the semi-microscopic mismatch and relaxation model of Funke, itself difficult to use for fitting of full complex data. Although the ZC model is superior to the AW one because it allows fitting of complex data, both lead to incorrect low-frequency-limiting $\sigma'(\omega)$ log–log slopes (termed just slopes hereafter) when σ_0 is subtracted from model response. The provenance of these models and reasons for their inadequacy are further described in [8].

The C symbol in the composite CK1S, CK0S, and CUNS complex-fit models of table 1 indicates the presence of a specific capacitance, of dielectric constant ε_x, in parallel with the bulk model. For the CK1 and CUN models, $\varepsilon_x \equiv \varepsilon_{D\infty}$, while for the K0 model it denotes ε_∞, the full limiting dielectric constant given by $\varepsilon_{C1\infty} + \varepsilon_{D\infty}$. Here $\varepsilon_{C1\infty}$ is an effective high-frequency-limiting dielectric constant associated entirely with ionic vibratory motion [2], zero in the absence of mobile charge. For the K0 model, the equivalent quantity, $\varepsilon_{C0\infty}$, is zero. In contrast, in the absence of dipolar dielectric dispersion in the frequency range of interest, $\varepsilon_{D\infty}$ is the endemic high-frequency-limiting bulk dielectric constant of the material, associated with multipole response. Failure to distinguish properly between $\varepsilon_{D\infty}$ and $\varepsilon_{C1\infty}$ is at the heart of the

incorrectness of using the K1 OMF electric modulus approach [12], rather than the CK1 one, for estimating and interpreting β_1 from $M''(\omega)$ modulus-level data. For fitting of $\sigma'(\omega)$ data, however, ε_x may be set to zero or held fixed and there is no difference between K1 and CK1 fit results at this level.

In figure 1, electrode polarization effects lead to a progressive decrease below σ_0 at sufficiently low frequencies, as is strongly apparent for materials 2, 3, and 6. Although negligible behaviour of this type appears in the low-frequency region for the single-crystal material-4 of the table, electrode polarization effects may also affect response in the high-frequency region [9, 10]. For material-4, their inclusion improved the UNS and K0S fits appreciably but not the AWS and ZCS fits, so only the AW and ZC results are shown for this material. Incidentally, when β_1 was taken as a free variable in K1S fitting of the material-4 data, the resulting estimated parameters differed little from those shown for the UNS fit because the estimated β_1 value was about 0.337, very close to 1/3. Note that all the estimated parameter values for the material-4 ZC and AW fits are the same, except for the τ_C ones, but slight differences appear for the corresponding estimates for ZCS and AWS fits. For ZC and AW fits of the same data, the τ_{AW} and τ_{ZC} quantities are related by $\tau_{AW} = \tau_{ZC}\cos(n\pi/2)$.

The K0 model is a direct Fourier transform to the frequency domain of conductive-system stretched-exponential temporal response. It is calculated numerically in LEVM. Its normalized form at the resistivity level is $I_0(\omega) = \rho_C(\omega)/\rho_0$ for the usual situation where $\rho_C(\infty)$ is zero or negligible. It follows that at the electric modulus level $M_{C0}(\omega) \equiv i\omega\varepsilon_V\rho_C(\omega) = i\omega\varepsilon_V\rho_0 I_0(\omega)$, and, because of a relation between the K0 and K1 distributions of relaxation times [3, 20], $M_{C1}(\omega) = i\omega\varepsilon_V\rho_0 I_1(\omega) = [1 - I_{01}(\omega)]/\varepsilon_{C1\infty}$. Here, $I_0(\omega)$ involves the K0 shape parameter β_0 while $I_{01}(\omega)$ is the same function but with the β_1 shape parameter. It follows from K1-model analysis that

$$\varepsilon_{C1\infty} = \sigma_0\langle\tau\rangle_{01}/\varepsilon_V \equiv \sigma_0\tau_{C1}\langle x\rangle_{01}/\varepsilon_V \tag{5}$$

where $\langle x\rangle_{01} = \beta_1^{-1}\Gamma(\beta_1^{-1})$, and Γ is the Euler gamma function. For $\beta_1 = 1/3$, $\langle x\rangle_{01} = 6$. For the K0 model, a similar expression is

$$\varepsilon_{C00} \equiv \varepsilon_C(0) = \sigma_0\langle\tau\rangle_0/\varepsilon_V \equiv \sigma_0\tau_{C0}\langle x\rangle_0/\varepsilon_V. \tag{6}$$

Here $\langle x\rangle_0$ is the same function as $\langle x\rangle_{01}$ but with β_1 replaced by β_0. Equations (5) and (6) then lead, for fits of the same data, to

$$\varepsilon_{C1\infty}/\varepsilon_{C00} = (\sigma_{01}\langle\tau\rangle_{01})/(\sigma_{00}\langle\tau\rangle_0) \approx \langle\tau\rangle_{01}/\langle\tau\rangle_0, \tag{7}$$

since σ_{01} and σ_{00} are nearly equal, for good fits.

Because of the wide applicability of the CUN model [20], it is valuable to take it as a standard for comparing with other fitting models. Therefore, the parameter estimates of a CUNS CNLS fit of the material-4 data were used to generate virtually exact UN and UNS $\sigma'(\omega)$ data sets for a wide radial frequency window extending from 10 r s^{-1} to 10^{13} r s^{-1}. In order to provide normalized K1 results applicable for arbitrary β_1 values, however, define $\theta_1 \equiv \omega\langle\tau\rangle_{01}$. Figure 2 shows how the logarithm of this quantity varies with D_σ for several choices. The top UN-model line of figure 2 approaches a limiting slope of $1/(1-\beta_1) = 3/2$ as D_σ increases. In order to estimate the width of a window in the frequency domain needed for a given value of D_σ, we can write, in the region where the limiting slope is a good approximation,

$$\omega_{max}\langle\tau\rangle_{01} \tilde{=} (\sigma'_{max}/\sigma_0)^{1/(1-\beta_1)}, \tag{8}$$

which allows an approximate value of ω_{max} to be estimated for a selected D_σ value and one of $\tau_{C1}\langle x\rangle_{01}$, equal to $6\tau_{C1}$ for the UN model. The approximation is quite adequate for $D_\sigma \geqslant 2$. Multiplication by $(1-\beta_1)$ for the β_1 values of 1/3 and 1/2 yields lines whose limiting slope is

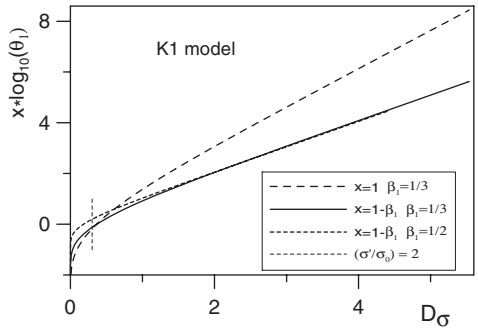

Figure 2. Curves showing the relationship between the normalized frequency quantity $\theta_1 \equiv \omega\langle\tau\rangle_{01}$ and the number of decades of variation of $\sigma'(\omega)$, $D_\sigma \equiv \log_{10}(\sigma'_{\max}/\sigma_0)$. Here and for use in subsequent figures, parameter estimates obtained from CUNS fits of the material-4 data identified in table 1 were employed to generate virtually exact UN and UNS $\sigma'(\omega)$ data sets for a wide radial frequency window extending from 10 to 10^{13} r s^{-1}.

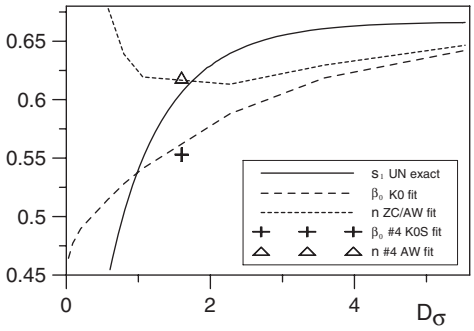

Figure 3. Slopes and exponents for exact UN-model data, and for K0 and ZC/AW-model fits of the UN data, versus D_σ. All such quantities, as well as $1 - \beta_1$, approach a limiting value of $2/3$ at high frequencies and large D_σ. Also shown are the corresponding table 1 values for fits of the material-4 data.

1, but it is clear that significant differences in the responses for these two values begin to appear for $D_\sigma < 1.5$, so equation (8) should only be used for larger values of D_σ. The vertical dashed line, for $\sigma'/\sigma_0 = 2$, is reached for the AW model when $\omega\tau_{\mathrm{AW}} = 1$.

3. Slopes, exponents, and range effects

High-frequency limiting slopes of $\sigma'(\omega)$ are important because they can often shed some light on which fitting models may be appropriate. Figure 3 shows how the slope of exact UN data, S_1, varies with D_σ and, through figure 2, with the available range of $\sigma'(\omega)$. Through the use of the results shown in figure 2 or equation (8), slope values can be related to the normalized frequency range θ_1. The high-frequency-limiting K1-model slope is $(1 - \beta_1)$ and that of the K0 model is just β_0. Thus for $\beta_1 = 1/3$, the UN model, and for $\beta_0 = 2/3$, the high-frequency-limiting values of S_0 and S_1 are both $2/3$.

A comparison of the approaches to $2/3$ for the K1 and K0 model slopes as a function of normalized frequency is presented in [20]. The high-frequency slopes of $\sigma'(\omega)$ data have been found, for a wide variety of materials, to be very close to $2/3$ (e.g., [20, 26], and the table 1 UN

fits herein), and CNLS fittings of such data generally show that the UN model yields better fits than does the K0 or the ZC.

The β_0 and n results in figure 3 are estimated values of these quantities, taken as free variables, obtained from K0 and ZC/AW fits of the present UN data but extending only up to a given D_σ value. They are thus slope or exponent estimates appropriate for fits of full but limited-range data. In contrast, the slope values of the S_1 curve are local values of the actual slope of the UN-model response at any point over the full range of D_σ. For example, $S_1 \cong 0.600$, 0.629, 0.655, 0.663, 0.665, and 0.666 for $D_\sigma = 1.5$, 2, 3, 4, 5, and 5.5, respectively. The two individual β_0 and n points shown in figure 3 were calculated from fits of the material-4 experimental data and, as expected, fall close to the curves based on fits of exact UN synthetic data.

As D_σ decreases, the fit of the K0 model to the UN-model $\sigma'(\omega)$ data progressively improves and its $100S_F$ value is less than 0.64 by $D_\sigma = 0.8$. Although the quality of ZC/AW fits also increases, its $100S_F$ fit-quality values remain much larger than those of the K0 fits in the small D_σ region, and for D_σ smaller than about 2, n itself changes in a direction opposite to that of S_1! As figure 3 indicates, the estimated value of n also approaches 2/3 appreciably slower for large D_σ than does the UN because of the failure of the AW/ZC model to provide a good fit in the mid-frequency range. ZC fitting of just higher-frequency data (data beginning at D_σ greater than 2 or 3) would, however, yield exponent values much closer to those shown for S_1. Incidentally, an earlier investigation of possible windowing effects with power-law models showed that reducing the frequency range of exact power-law data with random noise added did not appreciably affect the estimated values of the power-law exponent, n [27].

Not all $\sigma'(\omega)$ data lead to a limiting slope of 2/3, however. Slopes usually increase toward unity, may eventually exceed it, and at sufficiently high frequencies may approach a value of two before decreasing toward zero, yielding a plateau with a limiting constant value of $\sigma'(\omega)$. When this plateau is reached, ions vibrate and 'every hop or displacement of an ion is recorded individually and contributes to the conductivity' [19]. As shown in [6], either a non-zero value of $\rho_C(\infty)$ or the cut-off model, involving cut-off at a small τ value of the distribution of relaxation times associated with bulk response, can lead to a plateau. Although the plateau value thus need not involve a finite value of $\rho_C(\infty)$, it is the presence of such a finite value, not a cut-off, that leads to a slope of 2 before the plateau is reached.

It needs to be emphasized that even when the $\sigma'(\omega)$ slope is greater than either $(1 - \beta_1)$ or unity, fitting of such experimental data can still lead to well-determined estimates of bulk parameters, such as β_1, when appropriate fitting and analysis models are employed. Since electrode polarization effects, often well described by the SCPE model of equation (1), can contribute to both low- and high-frequency experimental response, it is worthwhile to investigate its high-frequency slope contributions for the UNS model.

It has been shown that the SCPE in conjunction with a bulk model can lead to conductivity slope values as large as $2 - \gamma_{SC}$ [28], and low-temperature material-4 experimental values as large as 1.7 have been observed and well fitted by the SCPE [9]. Although high-frequency NCL behaviour can also be fitted by a parallel constant-phase element (PCPE) [9, 10], most experimental ion-hopping data involve partial or complete blocking at electrodes or boundaries and can lead to significant low-frequency effects, as in the present figure 1. Since the PCPE model cannot describe such low- and high-frequency effects, it is plausible to use the SCPE even in those cases where a limited low-frequency range shows no deviation of $\sigma'(\omega)$ from a σ_0 plateau.

If one is interested in $\sigma'(\omega)$ data with slopes near unity, and thus of NCL character, it is appropriate to convert such a response to ε'' form, where constant loss, not physically allowable for a finite region, would yield a flat horizontal line in the frequency domain. Figure 4 shows

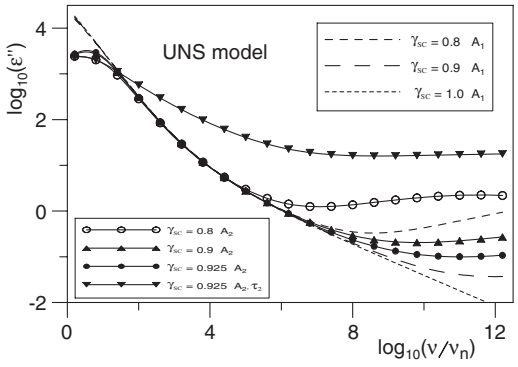

Figure 4. Log–log plots of the UNS-model dependence of the loss quantity ε'' on the frequency for several different bulk and electrode model parameter choices. Here A_1 is 100 times smaller than the original material-4 CUNS A_{SC} parameter value; A_2 is ten times smaller than A_1; and τ_2 is 100 times larger than the original τ_{C1} parameter value used here in calculating all other response curves but the one including τ_2. The normalization quantity ν_n is 1 Hz.

such results for exact UNS data with a variety of choices of UN- and S-model parameter values selected to demonstrate possible approaches to and deviations from NCL behaviour. The $\gamma_{SC} = 1.0$ curve is that for a pure ideal capacitance. Notice that the top line of the figure involves an NCL response whose actual slope varies only from about -0.02 to $+0.02$ over a range of nearly six frequency decades. The result is thus a good approximation to constant loss over many decades.

Recent work [29] demonstrates a connection between the magnitude of NCL and the activation energy associated with independent ionic hopping. If NCL is best described as a series effect, as discussed herein and usually associated with electrode polarization or sample boundary effects, such a connection would still be appropriate since the same mobile charges are involved in both long-range hopping and electrode polarization.

4. Hopping rates

In the Almond and West 1982–1983 bulk response fitting model (see the many references to it in [7]), they identified the parameter ω_{AW} of the present equation (3) as the thermally activated hopping frequency of the conduction process. Although there has been some uncertainty as to whether ω_{AW}, $\omega_{AW} = \nu_{AW}$, or $\nu_{AW} \equiv \omega_{AW}/2\pi$ should be designated the ion hopping frequency or rate [18, 30–32], actual fitting of equation (3) to appropriate data leads to an estimate of either ω_{AW} or $\tau_{AW} = 1/\omega_{AW}$, and so the numerical values of ω_{AW} obtained from such fitting will here be designated the hopping rate, of dimension r s^{-1}. This usage is consistent with the theoretically based discussion of hopping rate presented below.

The identification by Almond and West of ω_{AW} as the hopping frequency was purely empirical. It was considered and rejected soon after it was proposed [7], and in 1987 [33] and 1988 [34] its identification as a jump frequency or hopping rate was also independently termed inappropriate. Nevertheless, equation (3) and its estimation of a hopping rate have been widely used (e.g., [14, 17, 18, 30–32, 35, 36]). Therefore, it is worthwhile to discuss both a fitting model more appropriate than that of equation (3) and a solidly based expression for the hopping rate that can be estimated from such models as K1 and UN.

The Nernst–Einstein equation, appropriate when the fraction of available hopping sites occupied by mobile charges is small, may be written [6, 17, 18] as

$$\sigma_0 = [\gamma\lambda N(qd)^2/k_B T]H_R\omega_H, \tag{9}$$

where N is the maximum mobile charge number density; γ is the fraction of entities of charge q that are mobile; λ is a geometrical factor that depends on the dimensionality, D, of the space in which mobile charges are free to move and is given by $1/(2D)$; d is the rms single-hop distance for a mobile charge; k_B is the Boltzmann constant; H_R is the Haven ratio, $\leqslant 1$; and ω_H is the hopping rate, the inverse of a thermally activated hop time, τ_H. The Haven ratio was used in [17] but not in [6] or [18]. It was introduced to account for possible cross-correlation between successive charge jumps, but it is doubtful that it should be included in equation (9). For isotropic motion of charge carriers in three dimensions, $\lambda = 1/6$. In general, λ may be interpreted as associated with forward and backward charge motion along D orthogonal axes.

When estimated values of all the quantities in equation (9) but γN are available, it may be used to estimate this product. With the usual assumption of full dissociation of charges, $\gamma = 1$. Such estimation has been carried out in [17, 18], and [30] using results from equation (3) fit estimates of σ_0 and ω_{AW}. Their generally fairly close agreement with independent structural estimates of N led Dutta and Ghosh [32] to state that the results in [17] verify the assumption that ω_{AW} is the hopping frequency, but in their version of the present equation (9) they used $\omega_{AW}/2\pi$ rather than ω_H. Their claim is faulty, however, both because the arbitrary value $H_R = 0.5$ was used, and because of the empirical character of equation (3) itself.

Because of the generality and wide applicability of the K1 model, it is particularly plausible to accept its microscopic-based hopping rate, $\omega_H = 1/\langle\tau\rangle_{01}$, as that appropriate for any experimental data best fitted by the CK1 or CUN model. If one accepts this definition, then when one substitutes the σ_0 of equation (9) into equation (5), omitting the Haven ratio and taking $\lambda = 1/6$, it follows that [6, 10]

$$T\varepsilon_{C1\infty} = [\gamma N(qd)^2/6k_B\varepsilon_V]. \tag{10}$$

Therefore, for full dissociation when the quantity on the rhs of equation (10) and β_1 are both temperature independent, the activation energies of the thermally activated quantities $T\sigma_0$ and τ_{C1} are equal. Such exact equality is slightly challenged, however, when, as sometimes found experimentally, $T\varepsilon_{C1\infty}$ is not exactly temperature independent.

Define $r_R \equiv \tau_C/\langle\tau\rangle_{01}$ as a hopping time or rate ratio. For the AW model, it can be written as ω_H/ω_{AW}. Estimated values of r_R are listed for most of the materials in table 1 for AW fits. No values of r_R for ZC fits are listed in the table since they are of the order of twice those for the AW. Also, no r_R values are included for the Na_2SO_4 material because its K1-model β_1 values were very small, leading to very wide relaxation distributions and to consequent large uncertainties in the estimation of $\langle\tau\rangle_{01}$.

Figure 5 shows dependences of r_R on the logarithmic D_σ variable. Exact UN data, the same as those used in figure 3, were fitted by the ZC, AW, and K0 models and the resulting ratios shown in the figure. The K0 ones are included for comparison with the somewhat similar AW-fit ones. Note, however, that those involving $\langle\tau\rangle_0$ are not proper r_R results since $\langle\tau\rangle_0$ is not a K1 mean waiting time and, as shown in table 1, material-4 $\langle\tau\rangle_0$ results differ appreciably from the corresponding $\langle\tau\rangle_{01}$ values.

The individual material-4 experimental-data fit points shown in figure 5 lie close to the lines for the fits of the exact synthetic data, as expected for a situation where the UNS model is a good fit. The figure 5 results confirm that although ZC-model fits lead to very poor estimates of the proper mean waiting time and the mean hopping rate, those for AW fits are far superior but still mostly differ from $\langle\tau\rangle_{01}$ values by nearly a factor of two. Thus, since $\langle\tau\rangle_{01}$ values are a standard part of LEVM CK1 and CK1S fit results, there is no reason to use AW hopping time estimates in place of them.

An important aspect of hopping rate estimation is its use in calculating a value of the mobile charge carrier concentration N of equation (9). Such a calculation has been carried out

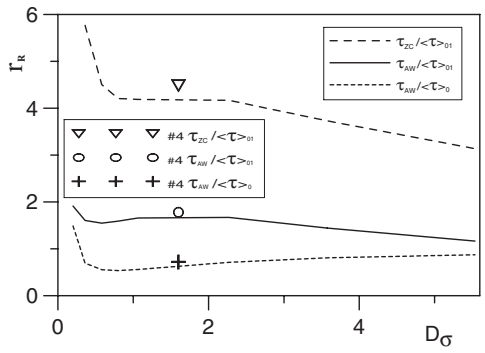

Figure 5. Dependence of the hopping time ratio, $r_R \equiv \tau_C/\langle\tau\rangle_{01}$, on D_σ for ZC, AW, and K0 fits of exact UN data. The $\tau_{AW}/\langle\tau\rangle_0$ results use the inappropriate mean hopping time $\langle\tau\rangle_0$.

for material-6, $PbSnF_4$, in [17], and its results will be compared with those for this material in table 1. Although the authors of this work fitted their 262 K data using the AW model of equation (3) with the SCPE of equation (1) in series, they found parameter estimates somewhat different to those listed in table 1. For easy comparison, values of the ρ_0, τ_{AW}, n, A_{SC}, and γ_{SC} parameters are listed below, first for the present AWS fit and then that from [17]:

$$3.497 \times 10^4,\ 2.518 \times 10^{-7},\ 0.657,\ 3.164 \times 10^5,\ \text{and } 0.959;$$

$$3.388 \times 10^4,\ 2.818 \times 10^{-7},\ 0.6,\ 4.484 \times 10^5,\ \text{and } 1.22.$$

The considerable differences between some of these estimates probably arose from the use in [17] of a form of the SCPE involving the expansion of $i^{\gamma_{SC}}$ as $\cos(\chi) + i\sin(\chi)$ with $\chi = \gamma_{SC}$ [30], rather than the proper $\chi = \pi\gamma_{SC}/2$.

In order to estimate values of N using the results of fitting the same data with two different fitting models whose results are identified with A and B subscripts, equation (9) leads to

$$N_A/N_B = (\tau_{HA}/\tau_{HB})(\rho_{0B}/\rho_{0A})[\gamma_B H_{RB}/\gamma_A H_{RA}], \tag{11}$$

where we shall initially take the quantity in brackets equal to one. If the subscript A denotes the AW model and B the K1 or UN one, then the first term in parenthesis on the right is just r_R. The value of the resistivity ratio is usually close to unity.

On assuming that $\gamma = 1$, $\lambda = 1/6$, $H_R = 0.5$, and $\omega_H = 1/2.818 \times 10^{-7}$ in equation (9), the authors of [17] estimated a value of N of about 1.798×10^{22} cm^{-3} and compared it with a structural value, N_S, of 1.994×10^{22} cm^{-3}. On correcting their estimate by replacing 2.818×10^{-7} by 2.518×10^{-7} and 3.388×10^4 by 3.497×10^4, one finds that equation (11) leads to a more proper AWS-model result of about 1.56×10^{22} cm^{-3}, less close to the estimated structural value. Similarly, the results in table 1 yield UNS and K1 estimates of about 1.02×10^{22} cm^{-3} and 1.65×10^{22} cm^{-3}, respectively. It is worth noting that for the present data set where D_σ is appreciably less than unity, even though the UNS, K1S, and K0S model fits led to comparable $100S_F$ fit quality factors, the relative standard deviations of the ρ_0 and $\langle\tau\rangle$ parameters were much larger for the K1S fit than for the others, making its listed r_R value quite uncertain.

It follows from the above results that $N/N_S \simeq 0.781$, 0.511, and 0.828 for the corrected AWS, UNS, and K1S fits, respectively. If we now change H_R from 0.5 to 1, these values change to 0.391, 0.256, and 0.414, all poor estimates. If one then assumes, for the sake of argument, that the actual conduction in the present material is one dimensional, the factor λ in equation (9) changes from 1/6 to 1/2, and the above results become 1.17, 0.768, and 1.24. But there seems no physically based reason here for this assumption.

The dissociation factor γ has been assumed to be unity for all the above calculations. Although it could be selected to make any of the above results that are less than 1 change to 1, one would expect γ to be temperature dependent if it were less than unity, yet the N estimates listed in [17] are very nearly independent of temperature. Thus the introduction of a temperature-independent $\gamma < 1$ factor seems unreasonable.

Finally, it should be noted that in [31] and [32] the ω_H of equation (9) is replaced by the ω_{AW} of equation (3) divided by 2π, converting it to a hopping frequency. If this factor were included, it would increase all the above results by 2π, still very poor agreement. But if one accepts equation (9) with $\omega_H = 1/\langle\tau\rangle_{01}$, a result following from the stochastic microscopic treatment of [22], there is no justification for the presence of the 2π factor in the Nernst–Einstein equation and in the estimation of values of N from it. Thus, for the present, it is unclear what changes would be required to allow a good estimate of N to be obtained using the microscopic mean waiting time for $1/\omega_H$, certainly a far more reasonable choice than $1/\omega_H = \tau_{AW}$. Analysis for data sets with larger values of D_σ and involving good UN-model fits should help clarify the situation.

5. Some non-universal responses

The Na_2SO_4 polycrystalline sodium sulfate results identified by 7 and 8 in figure 1 and in table 1 are included to illustrate data which cannot be well fitted by the UN model. This material undergoes a phase transition at about 513 K on heating from 461 K (phase V) and thus has a different structure at 540 K (phase I). Using equation (3), Ahmad [18] obtained n estimates of about 0.43 in the lower-temperature phase V region and about 0.61 for the higher-temperature region and concluded that they indicated the presence of low-dimensional and isotropic conduction processes, respectively. Although these n values differ from the corresponding AW ones shown in table 1, the two sets show the same trend. Note, however, that the table 1 K0-fit estimates of β_0 are nearly the same and close to $1/3$ for both phases. Further, no meaningful K1 fits were possible for either the phase-I or phase-V material because β_1 and τ_{C1} were so highly correlated that good estimates of both of them could not be obtained.

In recent work [37, 38] involving reference glasses and nanocomposites, ones whose data sets were limited to very small values of D_σ, such as those for the present material, it was found that CNLS CK0 fits of the reference data sets also led to β_0 estimates of exactly $1/3$ or close to that value. Taking account of the detailed structures of the materials involved, it was concluded that charge motion was constrained to one dimension, in agreement with a theoretical prediction of $1/3$ for such motion [20, 23].

The similarity of these fitting results to the present ones strongly suggests that charge motion in both the phase-I and the phase-V situations is one dimensional and remains so in spite of the effects of changing phase. This conclusion is speculative, particularly because D_σ is small for the present data sets, but if it is correct then the differences in n values for the two Na_2SO_4 situations should not be interpreted for such data as implying a change in charge-motion constraint.

Acknowledgments

The authors are grateful to all those who provided the data sets used in this study and to Professor A Ghosh for helpful comments.

References

[1] Macdonald J R 2004 *J. Appl. Phys.* **95** 1849
[2] Macdonald J R 2005 *Solid State Ion.* **176** 1961

[3] Macdonald J R 2006 *J. Phys.: Condens. Matter* **18** 629 (On the third line of p. 643 the word 'imaginary' should be replaced by 'real.')
[4] Macdonald J R 1998 *J. Appl. Phys.* **84** 812 (The word 'out' in the third line from the bottom of the first column of p. 820 should be 'but')
[5] Macdonald J R 1999 *Solid State Ion.* **124** 1
[6] Macdonald J R 2002 *Solid State Ion.* **150** 263
[7] Macdonald J R and Cook G B 1985 *J. Electroanal. Chem.* **193** 57
[8] Macdonald J R 2000 *Solid State Ion.* **133** 79
[9] Macdonald J R 2002 *J. Non-Cryst. Solids* **307–310** 913
[10] Macdonald J R 2005 *J. Phys.: Condens. Matter* **17** 4369
[11] Cole K S and Cole R H 1941 *J. Chem. Phys.* **9** 341
[12] Moynihan C T, Boesch L P and Laberge N L 1973 *Phys. Chem. Glasses* **14** 122
Moynihan C T 1994 *J. Non-Cryst. Solids* **172–174** 1395
[13] Sidebottom D L 2000 *Phys. Rev.* B **61** 14507
Sidebottom D L 2003 *J. Phys.: Condens. Matter* **15** S1585
[14] Bhattacharya S and Ghosh A 2005 *Solid State Ion.* **176** 1243
Bhattacharya S and Ghosh A 2005 *J. Phys.: Condens. Matter* **17** 5655
[15] Pimenov A, Ullrich J, Lunkenheimer P, Loidl A and Rüscher C H 1998 *Solid State Ion.* **109** 11
[16] Leon C, Santamaria J, Paris M A, Sanz J, Ibarra J and Varez A 1998 *J. Non-Cryst. Solids* **235–237** 753
[17] Ahmad M M, Yamada K and Okuda T 2004 *Solid State Ion.* **167** 285
[18] Ahmad M M 2005 *Phys. Rev.* B **72** 174303
Ahmad M M 2006 *Solid State Ion.* **177** 21
[19] Cramer C and Buscher M 1998 *Solid State Ion.* **105** 109
[20] Macdonald J R 2005 *Phys. Rev.* B **71** 184307
[21] Macdonald J R and Potter L D Jr 1987 *Solid State Ion.* **23** 61
Macdonald J R 2000 *J. Comput. Phys.* **157** 280 (The newest WINDOWS version, LEVMW, of the comprehensive LEVM fitting and inversion program may be downloaded at no cost from http://www.jrossmacdonald.com. It includes an extensive manual and executable and full source code. More information about LEVM is provided at this www address.)
[22] Scher H and Lax M 1973 *Phys. Rev.* B **7** 4491–4502
Scher H and Montroll E W 1975 *Phys. Rev.* B **12** 2455
[23] Macdonald J R and Phillips J C 2005 *J. Chem. Phys.* **122** 074510
[24] Macdonald J R 1996 *J. Non-Cryst. Solids* **197** 83
Macdonald J R 1996 *J. Non-Cryst. Solids* **204** 309 (erratum) (In addition, in equation (A2) G_D should be G_{CD})
[25] Macdonald J R 1997 *J. Non-Cryst. Solids* **212** 95 (The symbol σ should be removed from the right end of equation (12))
[26] Sidebottom D L, Green P F and Brow R K 1995 *J. Non-Cryst. Solids* **183** 151
[27] Macdonald J R 1997 *J. Non-Cryst. Solids* **210** 70
[28] Macdonald J R 2001 *J. Chem. Phys.* **115** 6192
[29] León C, Ngai K L and Rivera A 2004 *Phys. Rev.* B **69** 134303
[30] Hairetdinov E F, Uvarov N F, Patel H K and Martin S W 1994 *Phys. Rev.* B **50** 13259
[31] Ghosh A and Pan A 2000 *Phys. Rev. Lett.* **84** 2188
[32] Dutta D and Ghosh A 2005 *Phys. Rev.* B **72** 024201
[33] Jain H and Mundy J N 1987 *J. Non-Cryst. Solids* **91** 315
[34] Elliott S R 1988 *Solid State Ion.* **27** 131
[35] Ahmad M M, Hefni M A, Moharram A H, Shurit G M, Yamada K and Okuda T 2003 *J. Phys.: Condens. Matter* **15** 5341
[36] Yamada K, Ahmad M M, Ogiso Y, Okuda T, Chikami J, Miehe G, Ehrenberg H and Fuess H 2004 *Eur. Phys. J.* B **40** 167
[37] Gosh B, Chakravorty D, Macdonald J R and Das G C 2006 *J. Appl. Phys.* **99** 064307
[38] Basu S, Macdonald J R and Chakravorty D 2006 *J. Mater. Res.* **21** 1704